# Lawrence Berkeley National Laboratory
## Recent Work

**Title**
NUCLEATION OF SILVER (I) OXIDE INVESTIGATED BY SPECTROSCOPIC ELLIPSOMETRY

**Permalink**
https://escholarship.org/uc/item/9mp322s0

**Authors**
Mayer, S.T.
Muller, R.H.

**Publication Date**
1987-07-01

# Lawrence Berkeley Laboratory

## UNIVERSITY OF CALIFORNIA

## Materials & Chemical Sciences Division

Submitted to Journal of the
Electrochemical Society

**Nucleation of Silver (I) Oxide Investigated
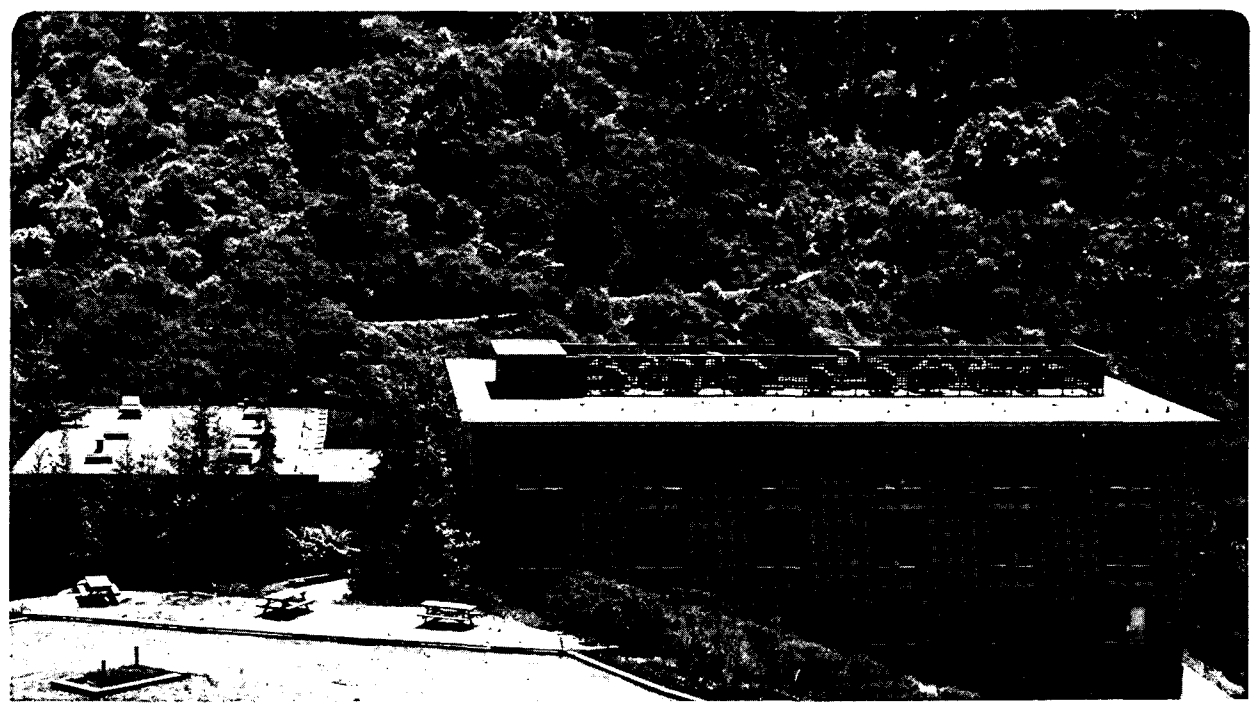by Spectroscopic Ellipsometry**

S.T. Mayer and R.H. Muller

July 1987

**For Reference**

Not to be taken from this room

## DISCLAIMER

# NUCLEATION OF SILVER (I) OXIDE

# INVESTIGATED BY SPECTROSCOPIC ELLIPSOMETRY

Steven T. Mayer and Rolf H. Muller

Lawrence Berkeley Laboratory

and

Department of Chemical Engineering

University of California

Berkeley, CA 94720

## ABSTRACT

The early stages of the anodic oxidation of Ag(111) in 1 M KOH during the application of potential steps, current steps and potential sweeps have been investigated by spectroscopic ellipsometry. Film thicknesses and surface coverage have been derived from the measurements by use of a dual-layer optical model. The results are supported by SEM observations on selected specimens. Oxide crystals are found to nucleate from a previously- formed homogeneous oxide layer. A decrease in number density of crystals of several orders of magnitude during film growth has been found and is attributed to the growth of larger crystals at the expense of smaller ones.

## INTRODUCTION

Theoretical models of electrocrystallization often assume either an instantaneous forma-
tion or a linear or exponential (progressive) increase in the number density of growth centers
with time [1]. More recent models have included the effect of a continuous decrease in the
number of available unnucleated sites as the surface becomes covered by crystals [2,3], the
potential dependence of the nucleation rate [2,3], a correction of the calculated surface cover-
age due to overlap [2,4] probabilistic time effects and the distribution of site energies [5]. All
the calculated current transients from these models are based on geometrical considerations
and the assumption that incorporation of reaction products at the crystal-electrolyte interface
is rate-controlling.

Silver has been chosen as a model system for the present investigation of the nucleation
and growth behavior of anodic films. While it is generally believed that the formation of the
silver oxide layer proceeds via a dissolution/precipitation mechanism, the course of events
leading to nucleation and growth of crystalline oxide has to be clarified. Time resolved Spec-
troscopic Ellipsometry has been used in combination with electrochemical measurements for
this purpose.

Wales and Burbank [6] showed in an x-ray diffraction study that the oxides of silver are
crystalline and that the formation of $Ag_2O$ preceded that of AgO during the anodic oxidation
of silver in KOH solutions. Based on x-ray diffraction, scanning electron microscopy (SEM)
and electron-diffraction measurements, Briggs et al. [7] described the morphology of the films
as multilayered. These experiments showed that an underlayer (called here the "primary
layer") forms first, followed by the formation of oxide crystals (secondary crystals) on top of
the primary layer. These results were later confirmed by an ellipsometric study [8].

A soluble silver species is believed to be responsible for a number of electrochemical
observation associated with the $Ag/Ag_2O$ system, despite the fact that silver oxide is known

to have a very low solubility ($10^{-5}$ M/l) in aqueous KOH solutions. Johnston et al. [9,10] proposed that the major soluble species at high pH is the $AgO^-$ ion, and this idea has been supported by a chemical stability study [11,12] and thermodynamic calculations. Various hydrated forms of this ion have also been proposed as the soluble species in the literature [13-15].

Cyclic voltammetry generally shows four characteristic anodic peaks for the Ag/KOH system; these peaks are referred to as A1 to A4. Only the first two (A1 and A2) are associated with the initial stages of $Ag_2O$ formation. The A1 (most cathodic) peak was originally identified by Dirske and De Vries [15], who reported a potential of formation of +95 mV versus Ag/AgCl 4 M KCl and assigned this peak to AgOH film formation, and a concurrent dissolution of the electrode. A number of other authors are in agreement with this general conclusion [12,16-20]. The formation of a soluble $AgO^-$ species prior to bulk oxide formation has been supported by the thermodynamic calculations of Pound et al. [12]. The A2 peak (200 mV vs. Ag/AgCl 4H M KCl) has been given various interpretations. Hampel and Tomkiewicz [21] attributed the A2 peak to the the "initial stages of oxidation". Hampson [22] explained the A2 peak as the preferential oxidation of surface atoms of low coordination numbers. Teijelo et al. [23] stated that the A2 and A3 peaks are due to different hydrates of silver oxide. Despite the numerous studies done on the $Ag/Ag_2O$ system, it is still unclear as to what physical or chemical processes lead to the various anodic cyclic voltammetry peaks.

## EXPERIMENTAL

A self-nulling spectroscopic ellipsometer with a 75 W xenon short arc white light source and a continuously variable interference filter [24,25] was operated at an angle of incidence of 75 degrees. Compared to a monochromatic measurement, a spectral scan of the surface represents a large number of independent measurements. Though an ellipsometer measures only two parameters at any wavelength, a spectral measurement makes it possible to determine more than two unknown quantities. Therefore, spectral measurements allow for the determination of a greater number of unknown optical quantities and for a greater certainty in those derived quantities. The instrument has been adapted to follow spectral changes in the optical properties of the surface with time [26,27]. The ellipsometer has a nulling time (ie. the time to make a measurement at one wavelength) of about 1 msec. One spectral scan (370-750 nm) provides about 40 independent measurements and requires about 3.5 seconds. The resolution of the present instrumental set-up used was 0.05 degrees for delta and 0.025 degrees for psi. Experimental data on wavelength, delta, psi and time are collected and stored by an DEC LSI 11/73 computer for later interpretation.

Electrochemical measurements were recorded on an EG&G model 273 potentiostat/galvanostat. This instrument was interfaced with a DEC LSI 11/73 for computer controlled potential programing and data transfer. The instrument also contains a digital coulometer.

A Teflon cell with two glass windows oriented normal to the beam was used. The cell had a volume of 244 ml and was equipped with ports for the introduction and removal of electrolyte and a nitrogen purge stream. The counter electrode was a platinum screen located 4 cm from the working electrode. A Ag/AgCl 4M KCl reference electrode (E=+205 mV vs. NHE) was connected to the cell by a capillary filled with 1 M KOH solution.

All measurements were made on in house grown single crystal Ag(111) surfaces. The surface area of the working electrode was approximately 3.6 cm$^2$. The surface preparation

involved a series of mechanical polishing step, ultrasonic cleaning and washing with a series of solvents increasing polarity. Next, the surfaces were chemically polished with a $KCN/H_2O_2$ solution. and the crystals were fitted into TFE holders. This surface preparation procedure was similar to that used before [8,28] and is described in detail elsewhere [26].

The electrolyte solutions (aqueous 1 M KOH) were pre-electrolyzed in an external Teflon cell containing two Pt electrodes held at a cell voltage of 800 mV. The electrolyte was then deoxygenated with nitrogen (99.99999% purity). Finally, the electrolyte was transferred to the nitrogen-purged optical cell. Before the experiment, the electrode was brought to a potential of -800 mV vs. Ag/AgCl for 15 seconds to remove any remaining surface oxides.

# MEASUREMENTS

Prior to every experiment the optical properties of the polished silver substrate in contact with 1M KOH were determined using the spectroscopic ellipsometer. The refractive index determined from that scan was later used in the data reduction. The values determined from clean surfaces were reproducible within a standard deviation over the spectrum of approximately 8% for n and 1.5% for k [26].

Due to the limited time resolution of spectral measurements, fixed-wavelength ellipsometry was used with cyclic-voltammetry at high sweep rate. Spectroscopic measurements were made concurrently with electrochemical measurements for current step, potential step and slow potential sweep experiments. These results all indicate that the anodic film formation can be separated into three regimes. The first regime is interpreted as the formation of a submonolayer to monolayer film. The second regime corresponds to the growth of a uniform multilayer film. The third regime is the nucleation and growth of oxide crystals at the surface.

### Potential Sweep

Simultaneous cyclic-voltammetry/fixed wavelength ellipsometer measurement were made at sweep rates ranging from 5 to 20 mV/second and with reversal potentials up to 200 mV. Figure 1 shows the changes in the psi parameter for one such experiment. Since the optical changes are quite small in this potential region only qualitative conclusions can be drawn and are summarized as follows. The total optical changes are smaller than those associated with a monolayer although the total charge passed is much larger than that necessary for a monolayer. The optical properties of the surface show immediate reversal upon cycle reversal, despite the fact that an anodic current continues to flow for a short time after cycle reversal. Further, we note that the rate of optical change is slower for the cathodic sweep than for the anodic sweep. We conclude from these observations that soluble anodic products

diffuse from the interface into the solution and that the ellipsometer detects a very thin layer which may be an adsorbed product which desorbs slowly. The dissolved material is not visible to the ellipsometer.

Transient spectroscopic ellipsometer measurements during a slow potential sweep are shown in figure 2. At this slow sweep rate there is very little change in the optical parameters up to a potential of 160 mV. Significantly larger changes occur in the potential range of 160-190 mV. Beyond the potential of 190 mV very rapid changes in delta and psi are observed. The current response for this sweep also shows three distinct regimes (figure 3). A very small current is observed at low potentials. A fourfold increase in the slope of the current curve is seen around 110 mV. At a potential of 185 mV, another change in slope is seen. At this potential the current increases dramatically. The optically observed changes coincide with changes in the current response. We associate these three regimes with the formation of a monolayer, the growth of a uniform multilayer, and the nucleation of surface oxide crystals.

### Current Steps

Spectroscopic Ellipsometer/Current step measurements were used to determine the relationship between the formation of the surface layers and the potential response. Current densities in the range of 50 to 200 $\mu A/cm^2$ were studied. Figure 4 shows the ellipsometer parameter $\psi$ for a series of scans made for an anodic current density of 75 $\mu A/cm^2$. In this figure the relative amplitude $\psi$ changes very little during an induction time of about 55 seconds but then undergoes rapid spectral dependent changes. The delta parameter also shows such an induction time. The induction time decreases with increasing current density. Model calculations (discussed in the next section) show that during the induction time a uniform multilayer is forming. The rate of its growth increases with current density. The rapid changes in optical parameters result from the nucleation process. Perhaps the most intriguing result of this

series of measurements is that, for the same charge passed, larger optical changes are seen at higher current densities. We interpret these trends as follows. At lower current densities, a greater portion of the oxidized material diffuses as a dissolved species from the interface. From the results discussed above, we believe that the formation of the primary layer may result from the accumulation of reaction products at the interface as the desorption/diffusion step in the overall reaction becomes slower than the rate of formation of anodic products. For this reason the current efficiency for the formation of the uniform layer ("primary layer") is low at low current densities. We postulate here that the formation of a critical thickness of primary layer oxide is necessary for the nucleation to occur. Therefore, at higher current densities where the current efficiency for primary layer film formation is greater, we expect nucleation to occur earlier (ie. at a smaller total charge passed). Once crystals are nucleated they can incorporate material which would otherwise dissolve into the electrolyte. Therefore, the nucleation results in a much greater overall current efficiency for film formation.

Typical polarization curves for galvanostatic oxidation [18,19,29,30] show a rising potential that peaks and then shows a shallow dip. Figure 5 shows potential measurements corresponding to the optical measurements shown in figure 4. An initial increase in potential is followed by a shoulder at around 200 mV, and then a plateau at 220 mV. This figure does not show any sharp decrease in potential after nucleation (occurring at approximately 60 seconds) as reported by Dignam et al. [29], though the potential did fall slightly for experiments performed at higher current densities. Most previous galvanostatic measurement were made at much higher current densities than studied here. After 220 seconds, the cell was set to open circuit.

### Potential Steps

The Ellipsometer/potential-step measurements were perhaps the most revealing. The monochromatic measurements show that very rapid changes in $\Delta$ and $\Psi$ occur during the first ½ second after the potential step is applied. Slower changes in ellipsometer measurements

follow and can therefore be monitored spectroscopically. The rapid change in $\Delta$ and $\Psi$ further indicates that the kinetics of the formation of the first monolayer is much faster than the subsequent film growth. This observation tends to support our hypothesis that slow desorption/diffusion of the reactant products from the interface leads to the the formation of the primary layer.

Spectral scanning was found to be effective for determining optical changes after the initial transient period. Spectral-ellipsometry results for a series of potential-step experiments show very slowly changing spectra in the range of 160-190 mV. For potential steps below 160 mV, no changes are found in delta or psi after the initial rapid change. For potential step larger than 200 mV, much more rapid changes in optical parameters are observed.

## OPTICAL MODEL

Several optical models were investigated in an attempt to reproduce the observed time-dependent spectroscopic ellipsometry measurements [26]. The optical model shown schematically in figure 6 was found to best represent the measurements. The film consists of two sub-layers. The layer closest to the substrate (primary layer) is a continuous homogeneous film. A second layer consists of an island film representing the optical effect of isolated secondary crystals by the coherent superposition of polarization states resulting from reflection on the islands and between them [26,31]. The free parameters of the optical model were the thickness of the first (primary) layer, and the thickness, coverage and solid fraction of the second layer (secondary crystals). The optical constants of the secondary crystals were considered an optical mixture of oxide and electrolyte. The Bruggeman Effective Media Model was used to determine the solid fraction of the crystals. The free parameters were derived from the measurements by multidimensional optimization with a SIMPLEX algorithm [27].

For the initial spectral scans (early times) the model parameters for the secondary layer were found to approach zero and the dual-layer model could be simplified to a single-film model. Under these conditions the film thickness and complex refractive index (assumed wavelength independent) of the oxide film were treated as free parameters and were derived from these measurements. The use of a wavelength-independent refractive index was sufficient to simulate wavelength-dependent ellipsometer measurements. Derivation of the wavelength dependent refractive index from the measurement of a growing primary layer showed very small spectral variations. The dual layer model was used when the introduction of the secondary crystal layer into the optical model gave none zero values of free parameters and the calculated spectra reproduced the observed spectra better than the simple single film model.

# INTERPRETATION OF MEASUREMENTS

## Potential Sweep

Below potentials of 130 mV, potential sweep ellipsometric data show that no film forms. Above this potential the surface coverage of a submonolayer film increases with applied potential and reaches full coverage around 160 mV. As the potential is increased further, a uniform multilayer (the primary layer) is formed with a thickness which steadily increases with potential until nucleation of the secondary layer occurs at around 200 mV. The growth rate of the secondary crystals (islands) calculated from the ellipsometric data does not vary greatly with potential.

## Current Step

As pointed out above, optical changes in galvanostatic experiments occur in two stages representing early thin-film growth (primary layer), and nucleation of surface crystals (secondary layer). The primary layer grows linearly with time and the rate increases with current density. The charge corresponding to the amount of material observed at the surface is much smaller than the total integrated current (only 10-25%). Secondary crystals are formed later. As the current density is increased, the time for the appearance of the crystals decreases. Figure 7 shows how the induction time for the onset of secondary film formation depends strongly on current density but that after nucleation the growth rate is almost independent of current density and time. From a charge balance calculation it is found that the current efficiency for film formation increases dramatically after the nucleation of secondary crystal.

## Potential Step

The ellipsometric responses to potential steps for this system fall into two classes; (1) Films containing only a primary layer and (2) Films which eventually nucleate secondary cry-

stals. Figure 8 shows a linear relation between the primary film thickness and the square root of time for a number of different potential step experiments. The growth rate constant ( $A^\circ$ $sec^{-1/2}$ ) increases with potential between 160 to 190 mV. Parabolic growth behavior in a potential step experiment is indicative of film formation controlled by diffusion through the growing layer. An extrapolated 4-5 A film is found at zero time. This finding is consistent with the hypothesis of very rapid monolayer growth followed by much slower primary layer growth. Charge balance calculations show that only a small fraction (10-20%) of the total charge appears in the form of a surface oxide for these primary layer films. Table 1 show the derived optical constants from a potential step experiment. The constant value of n and k with increasing thickness indicates that the film is growing uniformly.

Crystalization of the anodic products is observed for potential steps above 200 mV. Figure 9 shows calculated and measured $\Delta$ and $\Psi$ spectra for a 200 mV potential step. The spectra calculated from the dual-film model fit the observed spectra quite well considering the simplicity of the model and the complexity of the surface (see SEM photograph, figure 12). The model does not consider the fact that the crystals are not totally planar (parallel to the metal surface) and that they show a distribution of thicknesses. Indeed, if allowances are made for the size distribution of crystals [26], a significantly better fit of the observed spectra can be obtained. However, there is a loss of clarity and an increase in the uncertainty in the interpreted physical parameters when this is done. Also, large increases in computation time result from this approach since an integration of the optical response over crystal sizes is required inside the optimization routine.

Current transient measurements for potential-step experiments have been reported before [16,19,21,32,33]. Generally, these responses show current transients falling with time. Pound et al. [19] have reported that the current increases with the inverse square-root of time, indicating that the reaction is controlled by the one dimensional diffusion of a soluble species. At higher potentials a transient minimum and maximum have been reported [19,21].

However, while a number of authors have attributed the current transient peak to the formation of a surface phase, the role of several simultaneous processes (eg. dissolution, incorporation of material into growing crystals, changing surface coverage, crystal overlap) on the current response has not been adequately discussed in the literature.

The current responses for two potential step experiments are shown in figure 10. Below the nucleation potential (figure 10A), the current transients generally follow a Cottrell inverse square-root of time dependence, indicating one dimensional diffusion control of a soluble silver species [26]. After application of a potential step to the nucleation potential (figure 10B) a current minimum is observed.

# SUPPORTING MEASUREMENTS

Cyclic-Voltammetry and potential-ramping experiments were performed to obtain an overview of the specific events that occur during the anodic and cathodic processes and to associate various anodic peaks found in cyclic voltammograms with physical or chemical processes of the $Ag_2O$ system. It has been reported [34] that cyclic-voltammetry results are specific to crystal orientation. Results obtained here pertain only to the Ag(111) face.

A window opening voltammogram was performed to help correlate the optical results discussed above with voltammetric results. Figure 11A shows a window opening cyclic voltammogram to a peak potential of 170 mV. These results show no clear anodic peaks. Droog [34] also found no distinct anodic peak in this potential range for the Ag(111) surface. The waves in this cyclic voltammogram are similar in form to those generated by Casadio [35] for reversible anodic dissolution of electrode material inhibited by a redox adsorption/desorption process. The data are therefore consistent with our interpretation that in the potential region in which the monolayer films are formed, most of the anodic products diffuse from the interface, and that this process is rate limited by desorption.

If one continues to sweep to higher anodic potentials a cycle-dependent waveform develops (Figure 11B). The cathodic wave shows a very broad peak whose location moves to lower potentials with increasing reversal potential (and cycle). This is the occurrence of the C2 process. The anodic current wave increases (the current is greater at the same potential) as the reversal potential is increased. In this experiment, a complete voltammogram was developed up to 500 mV. This voltammogram is similar to those reported in the literature. However, if we now cycle in the A1 potential region we observe clear anodic and cathodic peaks, similar to those generally found for polycrystalline silver (Figure 11C). The size and appearance of the A1 peak is known to depend on the crystal face, with the Ag(110) face being more reactive than the Ag(111) [34]. Therefore, restructuring of the electrode surface occurs after the reduction of oxide from surface oxide crystals at a potential around 200 mV

vs. Ag/AgCl 4 M KCl. We therefore conclude that the A1 peak is associated with the diffusion of a soluble Ag species and the formation of the primary layer. It is the formation of the crystalline oxide which gives rise to the A2 and C2 peaks in the cyclic voltammogram.

Scanning electron micrographs were taken after anodization of silver to 1) observe the micromorphological structure of the thin films 2) to aid in the choice of an optical model and 3) to compare ellipsometric results with electron-microscope results where it was possible. The anodization process was interrupted at various times after the potential step to determine changes at the surface with time. SEM shows that prior to the current minimum of a potential step experiment no surface features are discernable. Beyond this points, crystal are observed which grow with time (figure 12a). The secondary crystals account for most of the surface material, and show preferential orientation of (111) planes on these Ag(111) surfaces. The number density and surface coverage of secondary crystal can be determined from these photographs and compared to number densities derived from ellipsometric calculations (table 2). The results and trends are in reasonable agreement with each other. Very slow potential sweeping anodization (<0.5 mV/sec) or anodization by a series of small potential steps causes a small number of very large crystals to be formed (figure 12b). The surfaces anodized in this manner gave the best SEM images. These surfaces showed three distinct silver oxide crystal structures. Small (<30 nM in diameter), high number-density crystal exist below a layer of larger, lower number density crystals. The larger crystals (secondary crystals) also show a layer of smaller crystals (tertiary layer) on top of them. This morphological structure has been reported earlier by Briggs et al [7]. The small crystals under the larger ones are not apparent in other SEM photographs and may be associated only with very slow anodization.

## DISCUSSION AND CONCLUSIONS

The fact that the growth rate of the secondary crystals was found not to be a strong function of potential for all of our experiments indicates that the overall reaction is controlled at the oxide/electrolyte interface rather that at the metal-oxide interface. Because of an

observed lack of shape or size dependence on applied potential, Briggs et al. [7] also concluded that the overall kinetics was not controlled by the kinetics at the metal-oxide interface.

Figure 13 shows the time dependence of the primary and secondary layer thicknesses derived from the spectral ellipsometry measurements after application of a 200 mV potential step. Application of a potential step above the nucleation potential does not result in immediate nucleation. The thickness of the primary layer increases initially but decreases sharply at the time of nucleation of the secondary layer. The initial thickness of the secondary crystal layer is nearly the same as that of the primary layer prior to nucleation. Classical dissolution/precipitation theory proposes that nucleation occurs from a supersaturated solution in the vicinity of the electrode surface. When the free energy (activity) of the soluble species at the surface surpasses a critical energy for the formation of stable nuclei, nucleation of crystals at the surface will occur. If nucleation occurred directly from a supersaturated solution, no induction time would be expected under potentiostatic conditions. The surface concentration (controlled by the potential) would not change with time and only instantaneous nucleation could be predicted on that basis. Therefore, the induction time for nucleation does not represent the time necessary to reach a given supersaturation (as previously believed), but results from the formation of the primary layer of a critical thickness which seems to be a necessary precursor for the formation of the crystalline layer.

Two additional parameters, the surface coverage of crystals and their solid fraction, are also derived from the measurements. The results indicate that the surface coverage of the crystals **decreases** rapidly during the early growth stage (figure 14). Later, the surface coverage increases slowly with time. The number density of crystals can be derived from the ellipsometer measurements of thickness and coverage under the assumption of a geometrical shape for the crystals (hemispherical used). Figure 15 shows the number density of crystals as a function of time thus derived for a galvanostatic experiment at 0.10 mA/cm$^2$. There is an unexpected **decrease** in the number density of several orders of magnitude during the period

of early growth. These results are significantly different from the assumptions used in past theoretical treatments. During the early growth stages, the crystals can be expected to be unstable, and oxide material may redistribute among crystals of different size with the larger crystals absorbing material from the smaller ones thus decreasing the total number of growing centers. Later, when these size effects are no longer important, the number density becomes time invariant.

The calculated solid fraction (a measure of hydration) decreases after the coverage has fallen. This may be due to a chemical transformation, or an optical averaging with electrolyte which surrounds the growing crystal.

One of the most frequently cited mechanisms for the formation of silver oxide has been the dissolution/precipitation mechanism. In this mechanism Ag dissolves and then reacts with water. The formation of an oxide film occurs by the precipitation of the dissolved material from a supersaturated solution. The overall reaction could be controlled by various steps in the reaction kinetics or the transport of materials. When a charge-transfer process associated with the formation of the ionic species is rate-determining, a Butler-Volmer equation should predict the current/potential characteristics of the system. If diffusion from the interface to the bulk solution is the major controlling factor, standard diffusion equations can be used to reproduce the observed current responses. On the other hand, when the reaction is controlled at the solution/crystal boundary, the process may be controlled by either the diffusion to the crystal or incorporation into the crystal lattice.

Volmer has said [36] that the work needed to form a critical nucleus in a supersaturated-solution is lowered by phase boundaries. Stranski [37] discussed the nature of crystal formation and talked of the stability of small nuclei in equilibrium with the supersaturated solution. He proposed that embryonic nuclei form in an adsorption layer, driven by surface diffusion.

The physical mechanism of film formation can be inferred from our results presented above. Figure 16 is a schematic of what we propose for the mechanism of film formation. An initial monolayer (a) forms very rapidly, followed by the much slower growth of a compact multilayer (b), the primary layer. Concurrent with the film formation process is the diffusion of a soluble oxidized species (c) into the electrolyte, and this material accounts for most of the oxidized material generated at low potentials. For potential-step experiments, the uniform multilayer grows according to a parabolic growth law, indicating diffusional control of film growth. At sufficiently high overpotentials, the multilayer grows to a critical thickness (100-200 $A^{\circ}$), where the oxide material (in the primary layer) can form a large number of small seed nuclei (d), and achieve a thermodynamically more favored state. During the initial stages of crystal growth, these secondary crystals grow by the transfer of oxide material from the primary layer. Crystals which formed earlier than others will be larger. Because the solubility of crystals increases with decreasing size (Gibbs-Thompson equation), large crystals (e) tend to act as sinks near smaller crystals (f), causing the total number of crystals to decrease. In solutions this phenomenon is commonly referred to as Oswald ripening. Calculation of size redistributions during homogeneous nucleation for electrochemical systems have been presented by Kappus [38]. As the larger crystals continue to grow they eventually reach a dimension where the size effects on solubility are no longer important and the number density become invariant with time (g). The primary layer grows to a thickness comparable to that before nucleation (h). Therefore, whereas diffusion through the solution appears to be the mechanism of material transport to the growing crystals, our results indicate that the nucleation and growth of silver oxide is far more complicated than that associated with the classical dissolution/precipitation mechanism.

This paper was presented at the October, 1986 meeting of the Electrochemical Society in San Diego, California. Abstract #506.

# ACKNOWLEDGMENTS

# REFERENCES

1. M. Fleischmann and H. R. Thirsk, "Metal Deposition and Electrocrystallization," in Advances in Electrochemistry and Electrochemical Engineering. Vol. 3. P. Delahay and C. W. Tobias, ed., John Wiley and Sons, New York, 1963.

2. E. Bosco and S. K. Rangarajan, J. Chem. Soc., Faraday Trans. **77,** 483 (1981).

3. H. Angerstein-Kozlowska, B. E. Conway and J. Klinger, J. Electroanal Chem., **87,** 301 (1978).

4. M. Y. Abyaneh, Electrochim. Acta., **27,** 1329 (1982).

5. S. Fletcher, Electrochim. Acta., **28,** 237 (1983).

6. C. P. Wales and J. Burbank, J. Electrochem. Soc. **112,** 13 (1965).

7. G. W. D. Briggs, M. Fleischmann, D. J. Lax, and H. R. Thirsk, Trans. Faraday Soc. **64,** 3120 (1968).

8. R. H. Muller and C. G. Smith. Surf. Sci. **96,** 375 (1980).

9. H. L. Johnston, F. Cuta, and A. B. Garrett, J. Am. Chem. Soc. **55,** 2311 (1933).

10. H. L. Johnston, F. Cuta, and A. B. Garrett, J. Am. Chem. Soc. **56,** 1250 (1934).

11. P. J. Antikainen, Sirkka Heitanen, and Lars Gunnar Sillen, Acta Chem. Scand. **14,** 95 (1960).

12. B. G. Pound, Digby D. MacDonald, and John W. Tomlinson, Electrochem. Acta **24,** 929 (1979).

13. R. D. Giles, J. A. Harrison, and H. R. Thirsk, J. Electranal. Chem. **22,** 375 (1969).

14. B. V. Tilak, R. S. Perkins, H. A. Kozlowska, and B. E. Conway, Electrochim. Acta. **17,** 1447 (1972).

15. T. P. Dirkse and Dale B. De Vries, J. Electroanal. Chem. **63,** 107 (1959).

16. J. M. Droog, P. T. Alderliesten, and G. A. Bootsma, J. Electroanal. Chem. **99,** 173 (1979).

17. R. D. Giles and J. A. Harrison, J. Electroanal. Chem. **27,** 161 (1970).

18. J. M. Droog, and F. Huisman, J. Electroanal. Chem. **115,** 211 (1980).

19. B. G. Pound, D. D. MacDonald, and J. W. Tomlinson, Electrochim. Acta. **25,** 563 (1980).

20. B. G. Pound, D. D. MacDonald, and J. W. Tomlinson, Electrochim. Acta. **25,** 1293 (1980).

21. M. Hepel and M. Tomkiewicz, J. Electrochem. Soc. **131,** 1288 (1984).

22. M. L. Hampson, J. Electroanal. Chem. **45,** 149 (1973).

23. M. L. Teijelo, J. R. Vilche, and A. J. Arvia, J. Electroanal. Chem. **162,** 207 (1984).

24. H. J. Mathieu, D. E. McClure, and R. H. Muller. Rev. Sci. Instrum. **45,** 798 (1974).

25. R. H. Muller and J. C. Farmer. Rev. Sci. Instrum. **55,** 371 (1984).

26. S. T. Mayer, M. S. Thesis, Dept. of Chemical Engineering, University of California, Berkeley. December 1985. Lawerence Berkeley Laboratory report LBL-15607.

27. S. T. Mayer and R. H. Muller, "Data Acquisition and Reduction Software for a Self-Nulling Ellipsometer". Lawerence Berkeley Laboratory report LBL-20677, Dec. 1985.

28. R. F. Steiger, J. M. Morabito Jr., G. A. Somorjai, and R. H. Muller. Surf. Sci. **14**, 279 (1969).

29. M. J. Dignam, H. M. Barrett, and G. D. Nagy, Can. J. Chem. **47**, 4253 (1969).

30. B. D. Cahan, J. B. Ockerman, R. F. Amlie, and P. Ruetschi, J. Electrochem. Soc. **107**, 725 (1960).

31. R. H. Muller and J. C. Farmer. Surf. Sci. **135** 521 (1983).

32. M. Fleischmann, D. J. Lax, and H. R. Thirsk, Trans. Faraday Soc. **64**, 3128 (1968).

33. B. G. Pound, D. D. MacDonald, and J. W. Tomlinson, Electrochim. Acta. **25**, 1293 (1980).

34. J. M. Droog, J. Electroanal. Chem. **115**, 225 (1980).

35. S. Casadio, J. Electroanal. Chem. **67**, 123 (1976).

36. M. Volmer, Die Kinetik der Phasenbildung, Steinkopff, Dresden und Leipzig, 1939.

37. I. N. Stranski, Naturwissenschanften, **23**, 144 (1943).

38. W. Kappus, Electrochim. Acta. **28**, 1529 (1983).

# TABLE I

## OPTICAL CONSTANTS ($\hat{n} = n - ik$) OF PRIMARY LAYER OXIDE AT VARIOUS THICKNESSES

| TIME (sec) | POTENTIAL * (mV vs. Ag/AgCl) | THICKNESS A ° | REFRACTIVE ** INDEX (n) | EXTINCTION ** COEFFICIENT (k) |
|---|---|---|---|---|
| 23 | 190 | 8.0 | 3.44 | 1.15 |
| 133 | 190 | 14.1 | 3.33 | 1.09 |
| 426 | 190 | 20.9 | 3.47 | 1.02 |
| 598 | 210 | 27.3 | 3.23 | 1.07 |
| 667 | 210 | 34.7 | 3.24 | 1.01 |
| 978 | 210 | 42.8 | 3.22 | 0.97 |

* 190 mV Potential Step (575 seconds), followed by a step to 210 mV
** Assumed wavelength independent

# TABLE II

| | | | |
|---|---|---|---|
| COMPARISON OF NUMBER DENSITIES OF $Ag_2O$ ON Ag DETERMINED BY SPECTROSCOPIC ELLIPSOMETRY AND SCANNING ELECTRON MICROSCOPY | | | |
| | TIME (sec) | ELLIPSOMETRY $cm^{-2}$ | SEM $cm^{-2}$ |
| Potential Step | | | |
| 220 mV | 131 | $5.4 \times 10^8$ | $3.4 \times 10^8$ |
| 200 mV | 175 | $4.5 \times 10^8$ | $2.9 \times 10^8$ |
| 200 mV | 285 | $4.3 \times 10^8$ | $2.1 \times 10^8$ |
| Current step | | | |
| 75 $\mu A/cm^2$ | 220 | $3.1 \times 10^8$ | $1.9 \times 10^8$ |
| 100 $\mu A/cm^2$ | 235 | $3.2 \times 10^8$ | --- |
| 200 $\mu A/cm^2$ | 106 | $6.8 \times 10^8$ | $4.0 \times 10^8$ |

## FIGURE CAPTIONS.

1) Ellipsometer parameter $\psi$ during a potential cycling. Peak potentials are -250 and 175 mV vs. Ag/AgCl 4M KCl. Scan rate 20 mV/sec, wavelength 514.5 nm, Ag (111) surface.

2) Transient spectroscopic ellipsometer measurements during a slow potential sweep (0.5 mV/sec). Measured changes for the original surface of $\Delta$ (A) and $\psi$ (B), and calculations for optical model (smooth curves). Potentials for different optical scans shown. Note that there are no changes below 110 mV, moderate changes up to 185 mV, and large changes above 185 mV. Ag (111) surface.

3) Current response to a potential sweep at 0.5 mV/sec (corresponding to ellipsometer measurements in figure 2). Electrode surface area 3.19 $cm^2$. Ag (111) surface. Changes in slope are observed at 110 and 185 mV.

4) Changes in the ellipsometer parameter $\psi$ during a 75 $\mu A/cm^2$ constant current experiment after 1) 55 seconds, 2) 84 seconds, and 3) 120 seconds. Ag (111) surface. Note small changes up to 55 seconds.

5) Potential change with time corresponding to ellipsometer measurement of figure 4. Ag (111) surface. Note shoulders in potential at 200 and 220 mV.

6) Schematic representation of optical model used to interpret ellipsometer measurements of anodic surface layers. Primary layer represented as a homogeneous non-porous oxide, secondary layer as a porous island oxide.

7) Increase of secondary crystal thickness with time derived from ellipsometer measurements for various constant current densities. A) 50 $\mu A/cm^2$. B) 75 $\mu A/cm^2$. C) 100 $\mu A/cm^2$. D) 200 $\mu A/cm^2$.

8) Increase of primary layer thickness with square root of time derived from ellipsometer measurements for various potential steps. 1) 160 mV. 2) 170 mV. 3) 190 mV.

9) Calculated and measured spectra of $\psi$ (A) and $\Delta$ (B) for a potential step to 200 mV (141 seconds, charge passed 12.7 $mC/cm^2$). Spectra of the film free substrate shown for comparison.

10) Current transients for potential steps to A) 200 mV and B) 190 mV versus Ag/AgCl 4M KCl. Electrode surface area 3.19 $cm^2$. Ag (111) surface.

11) Window opening cyclic voltammograms of Ag(111) surface, geometrical area 3.19 $cm^2$. A) Anodic reversal potential increased by 10 mV each cycle up to a reversal potential of 170 mV. B) Same as in A) with reversal potential up to 280 mV. Continued cycling by increasing potential 10mV up to a reversal potential of 500 mV results in previously published features (not shown). C) Window opening voltammogram of the cycled electrode in the same potential region as in A).

12) Scanning electron micrograph of anodized Ag (111) surface. A) Single potential step to 200 mV versus Ag/AgCl 4M KCl, 375 seconds, 37.5 $mC/cm^2$. B) Surface anodized by a series of three potential pulses. 10 minutes from -50 to 190, 10 minutes from 190 to 210 mV and 3 minutes from 210 to 230 mV. Total charge passed 41.7 $mC/cm^2$.

13) Thickness of primary or underlayer (A) and secondary or crystal layer (B) derived from

ellipsometer measurements for a film formed by a potential step at time zero to 200 mV versus Ag/AgCl 4M KCl. Note decrease of primary layer thickness at onset of secondary layer growth.

14) Fractional surface coverage by the secondary (crystal) layer derived from ellipsometer measurements for a film formed by a potential step at time zero to 200 mV versus Ag/AgCl 4M KCl. Note decrease in surface coverage during early crystal growth.

15) Number density of secondary crystals as a function of time as interpreted from ellipsometric measurements for a galvanostatic film growth at 0.1 mA/cm$^2$. Note large decrease during the early growth stage.

16) Schematic representation of the proposed film formation mechanism. (a) Initial monolayer. (b) Compact multilayer. (c) Soluble oxide species. (d) Crystal nuclei. (e) Larger crystals growing at expense of smaller crystals (f). Large secondary crystals (g). Resumed growth of primary layer (h).
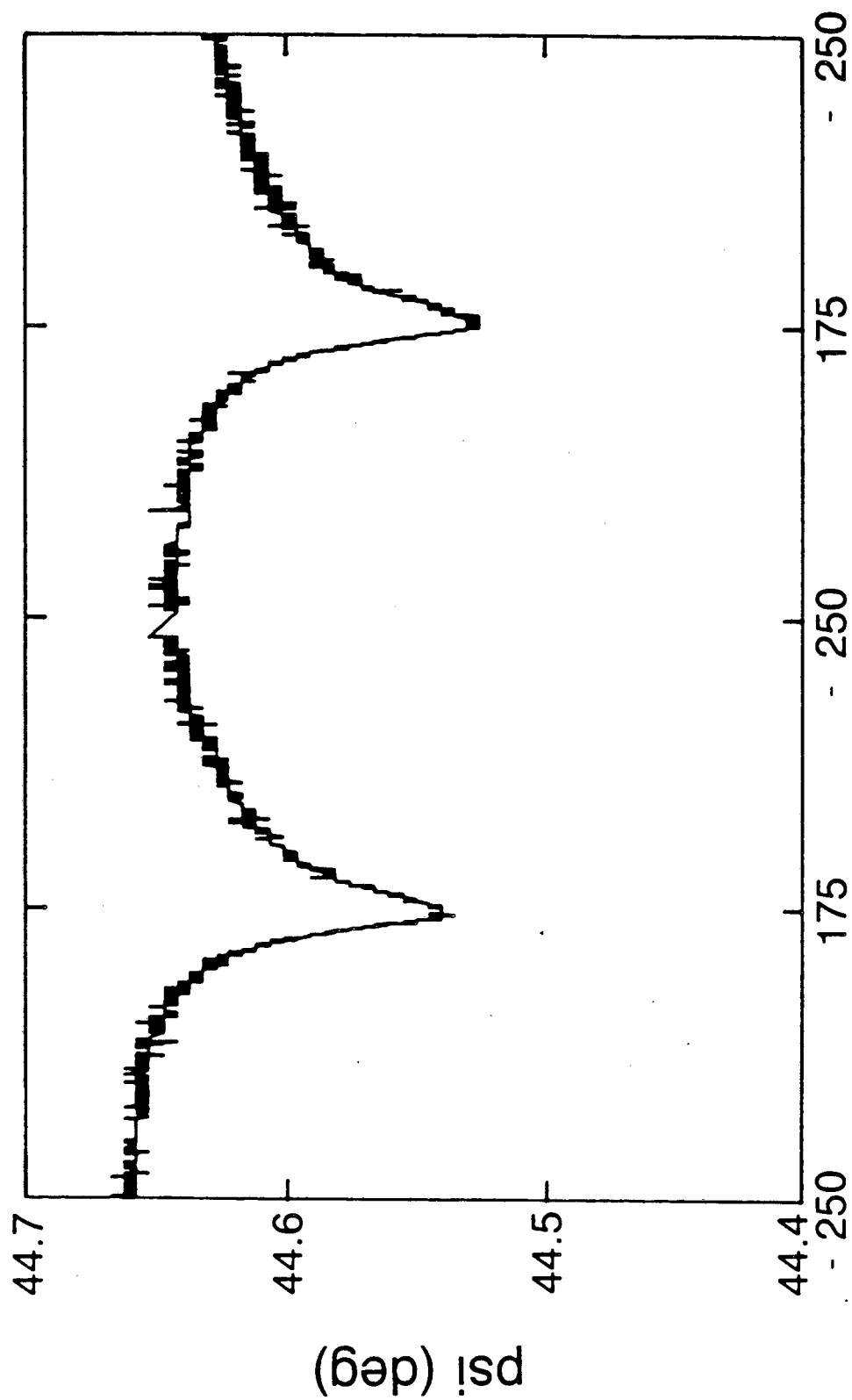
Fig. 1

XBL 8511-12725
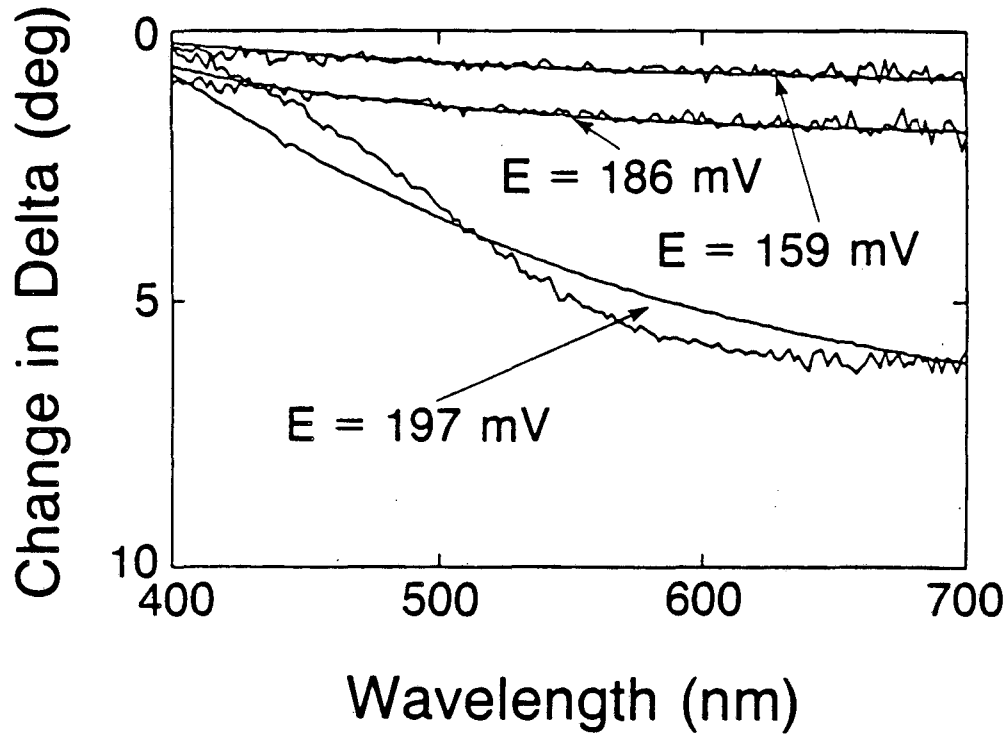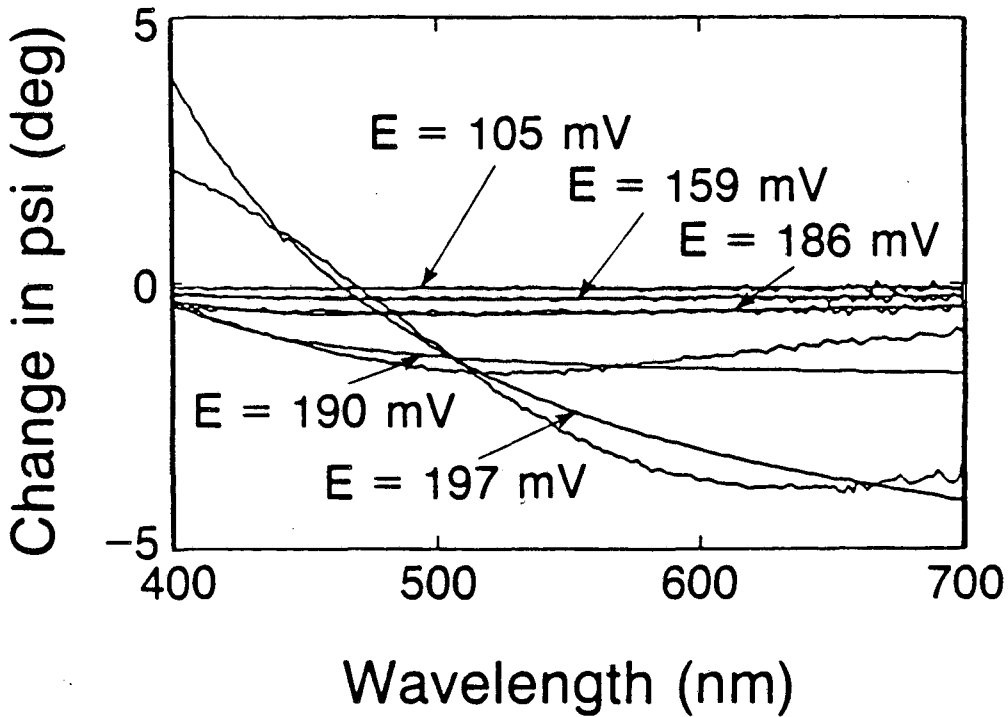
Fig. 2

XBL 8511-12751

Fig. 3

XCG 8511—479

XBL 8511-12719

Fig. 4

XCG 8511-478

Fig. 5

33



Porous Island Oxide

Non Porous Oxide

Substrate
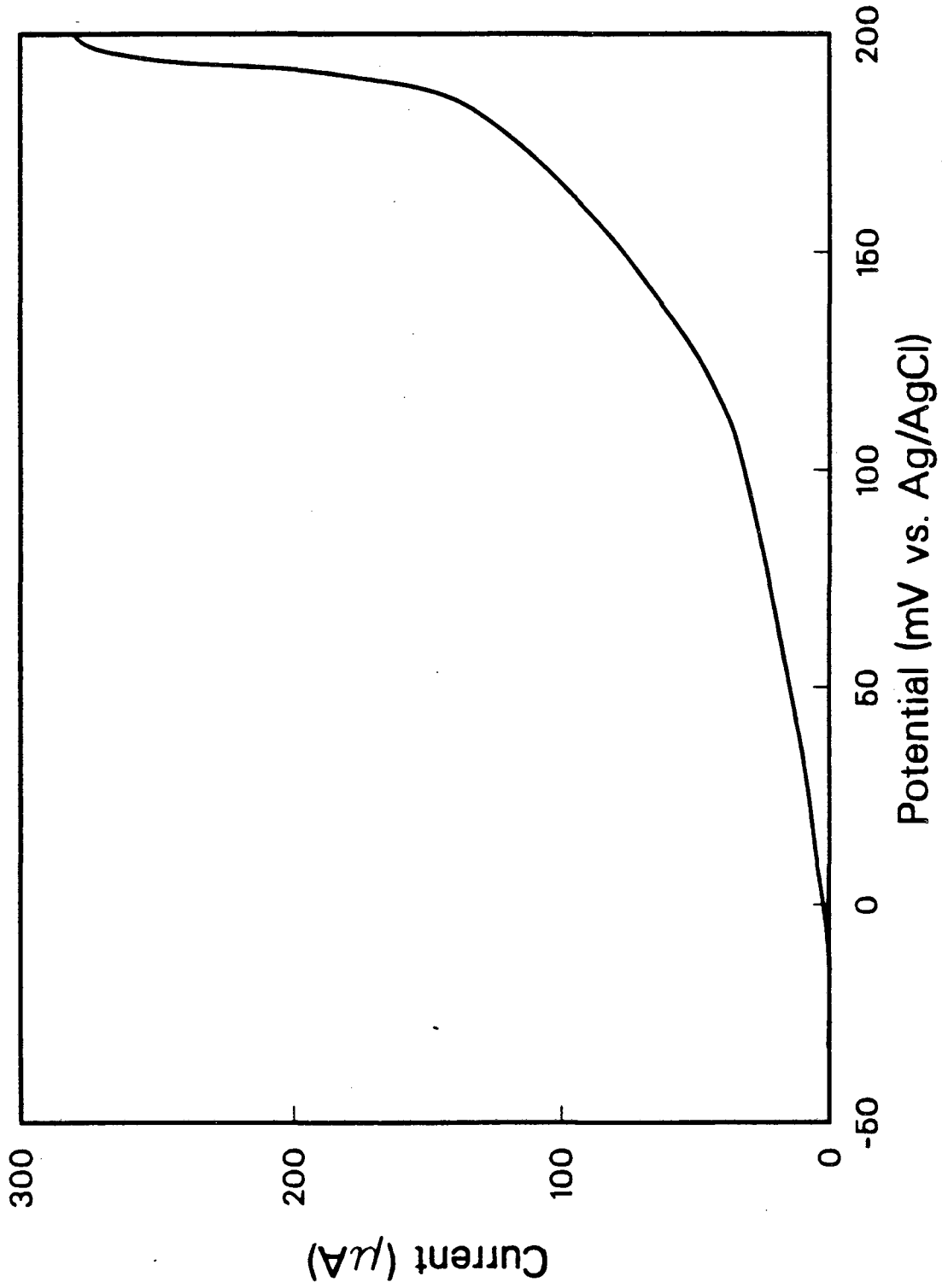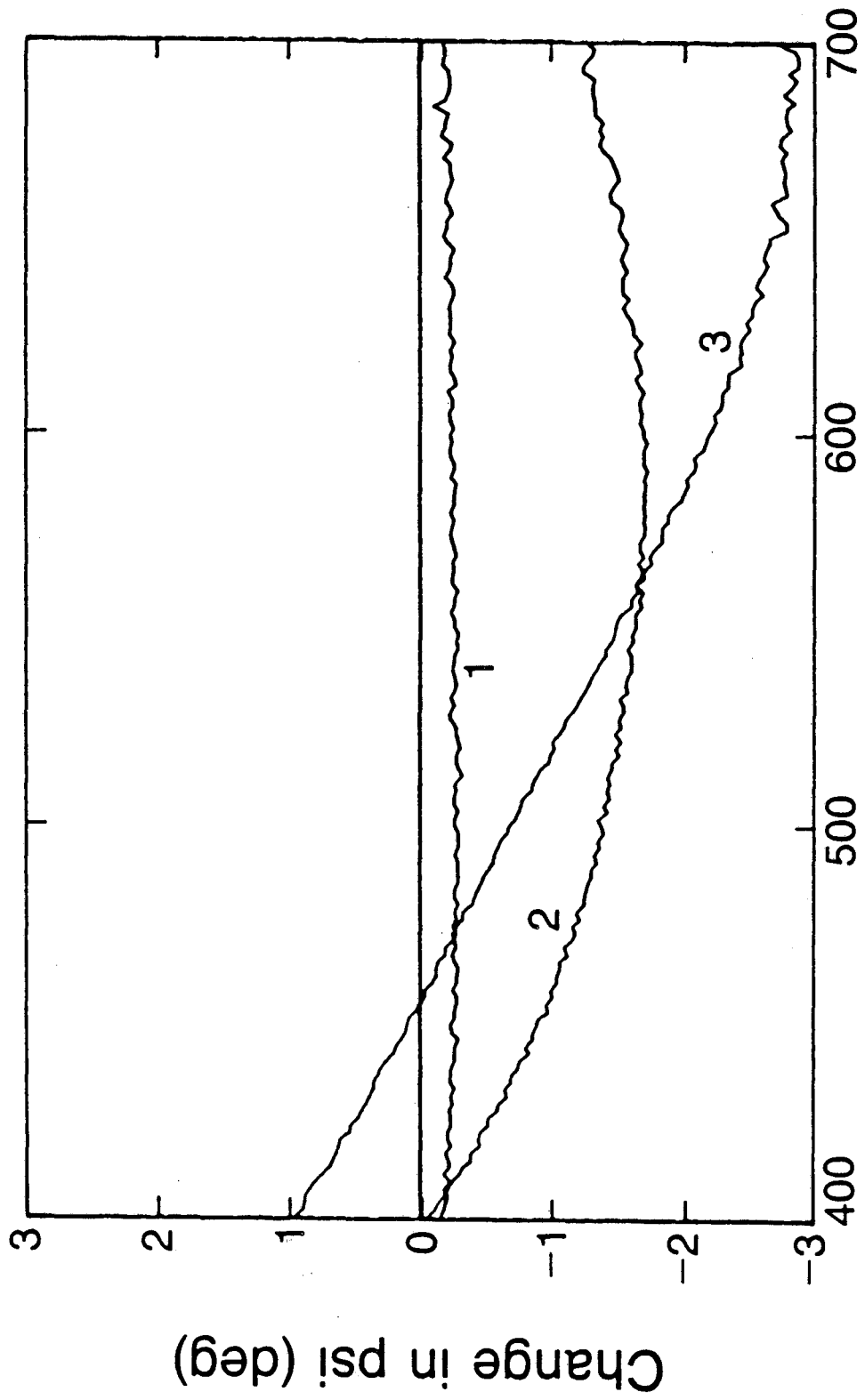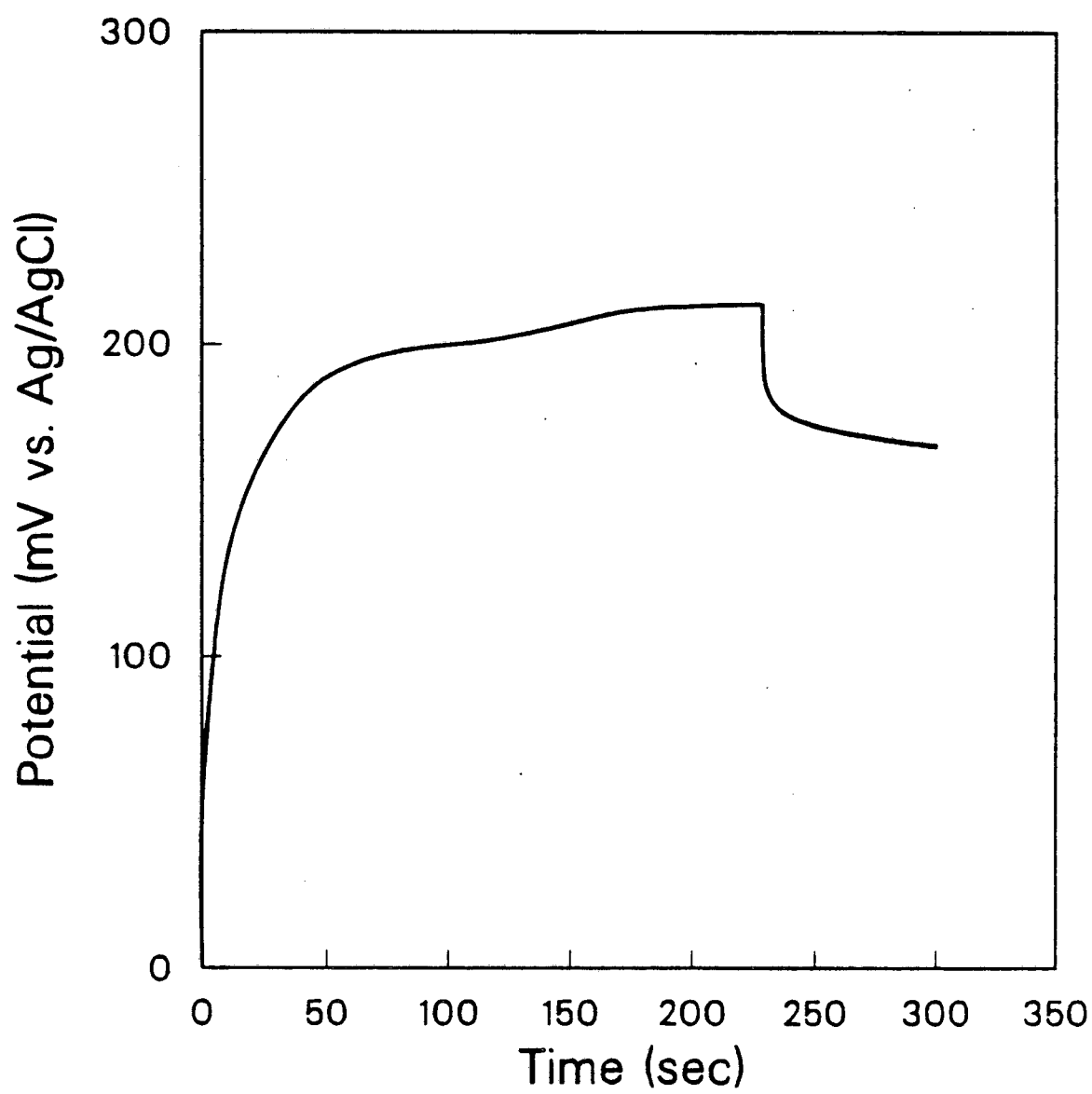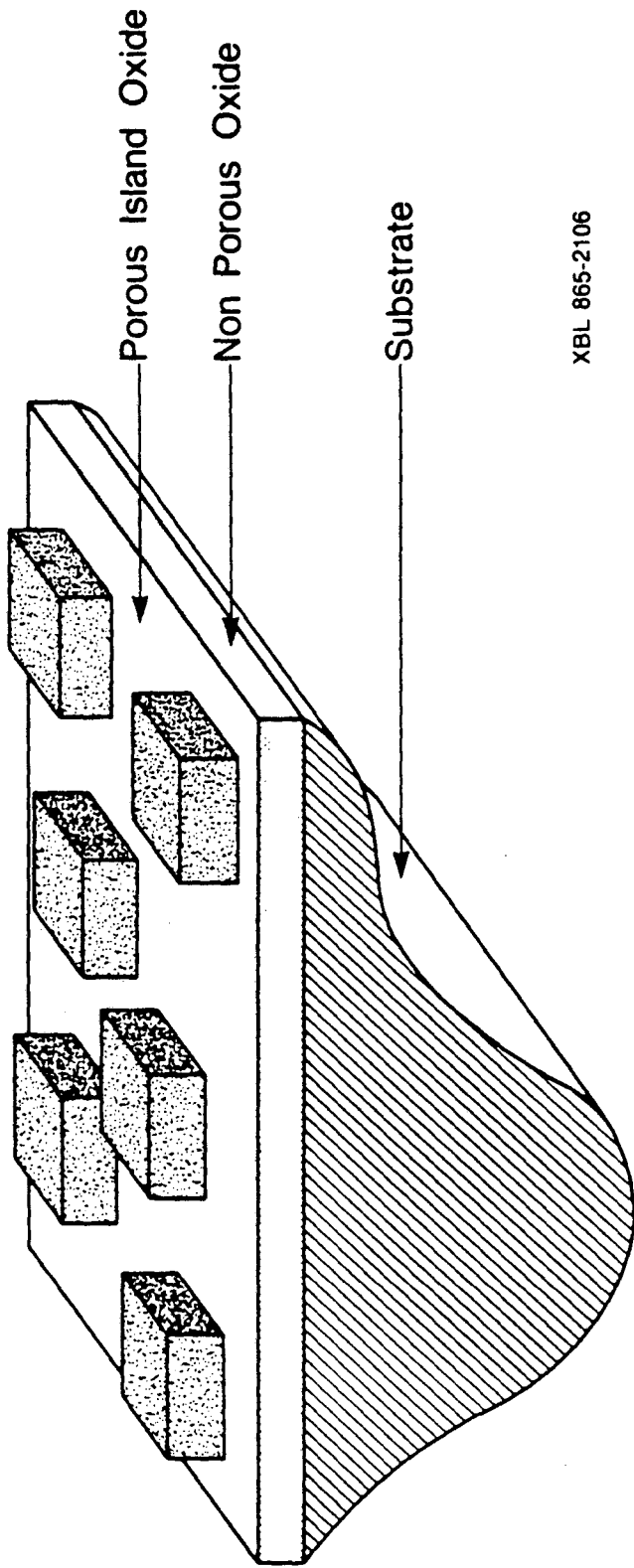
XBL 865-2106

Fig. 6
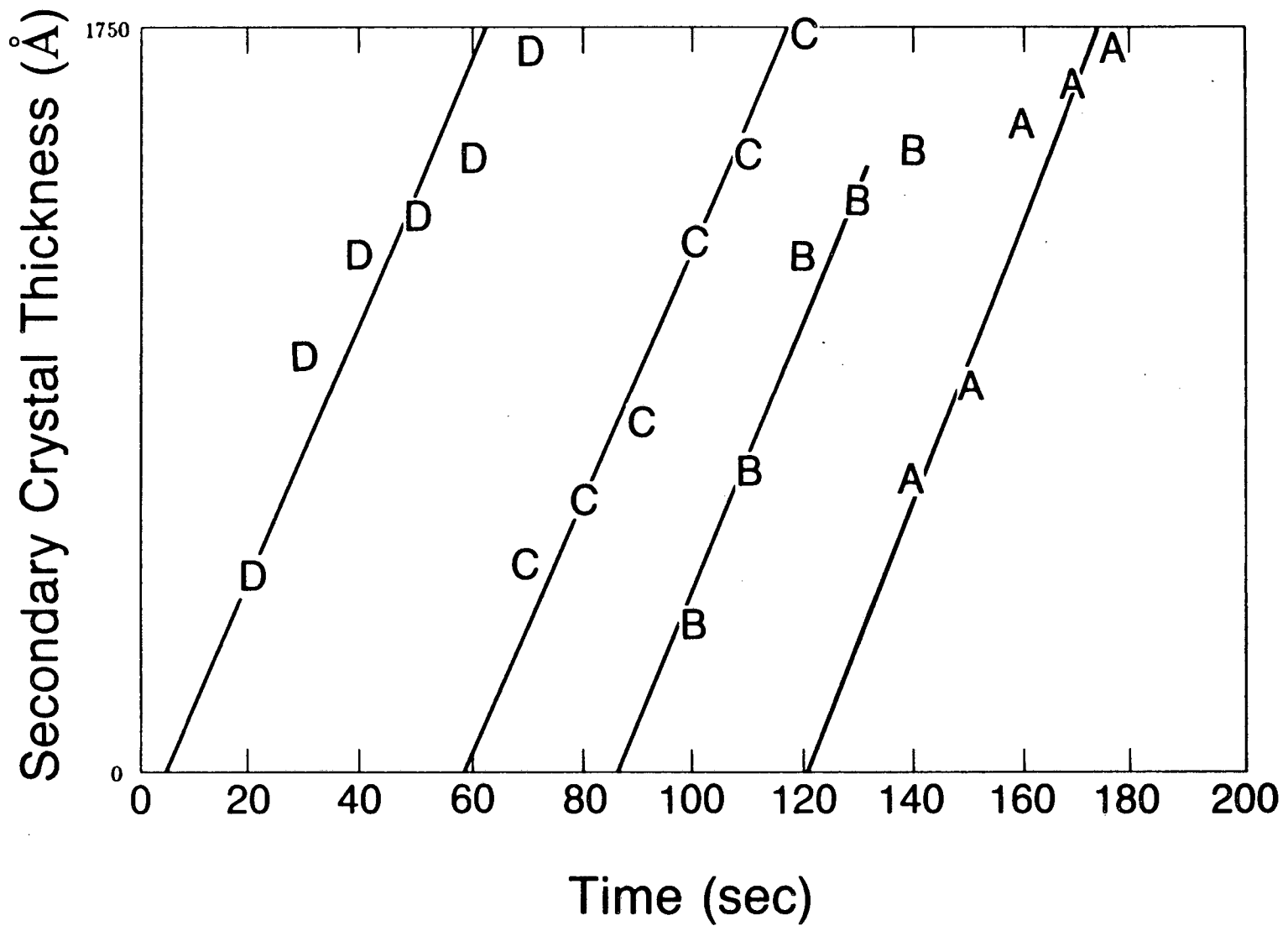
Fig. 7

XBL 8511-12742

34
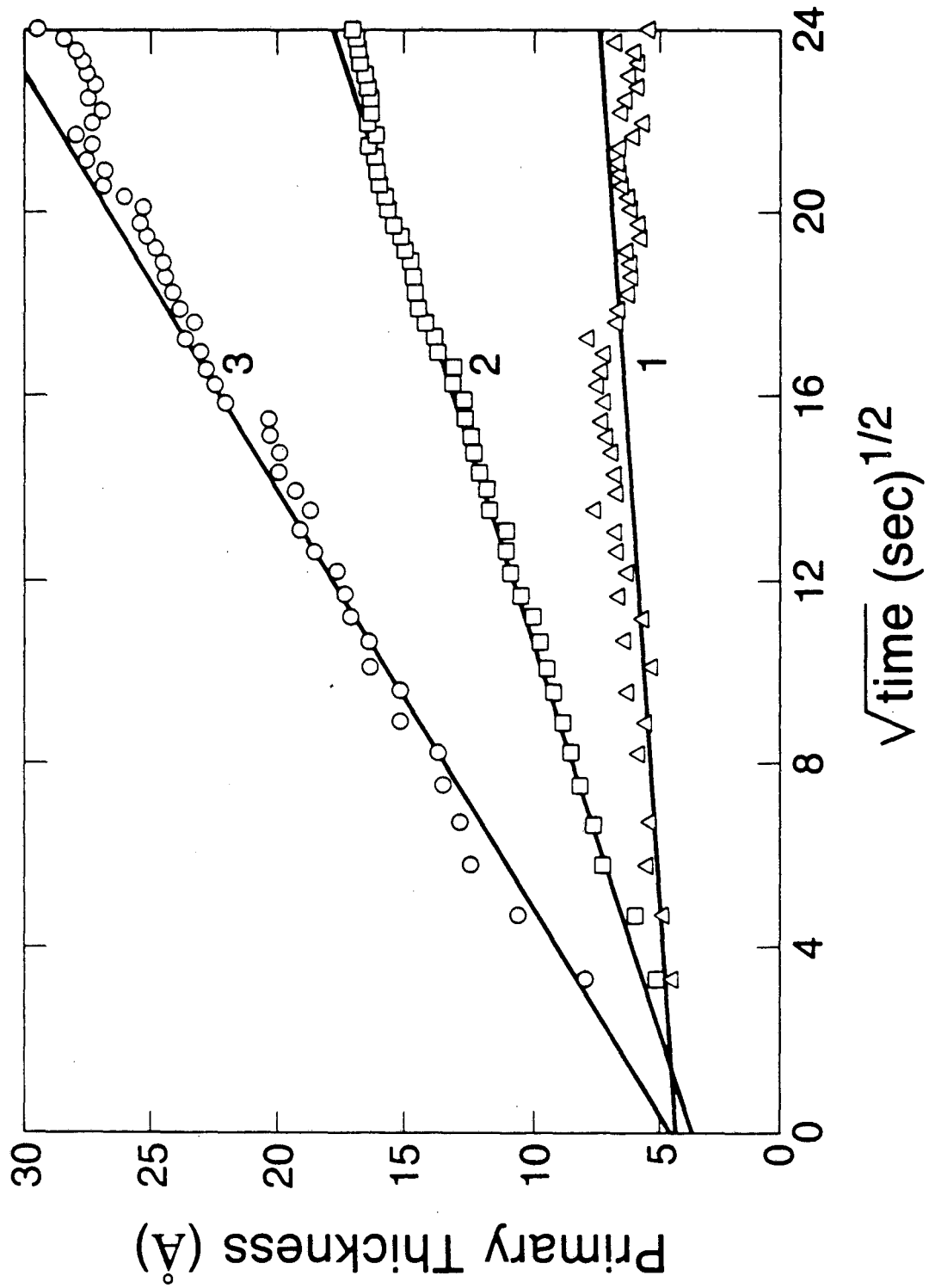
Fig. 8

XBL 8511-12752

A



XBL 8511-12740A

B

Fig. 9

37
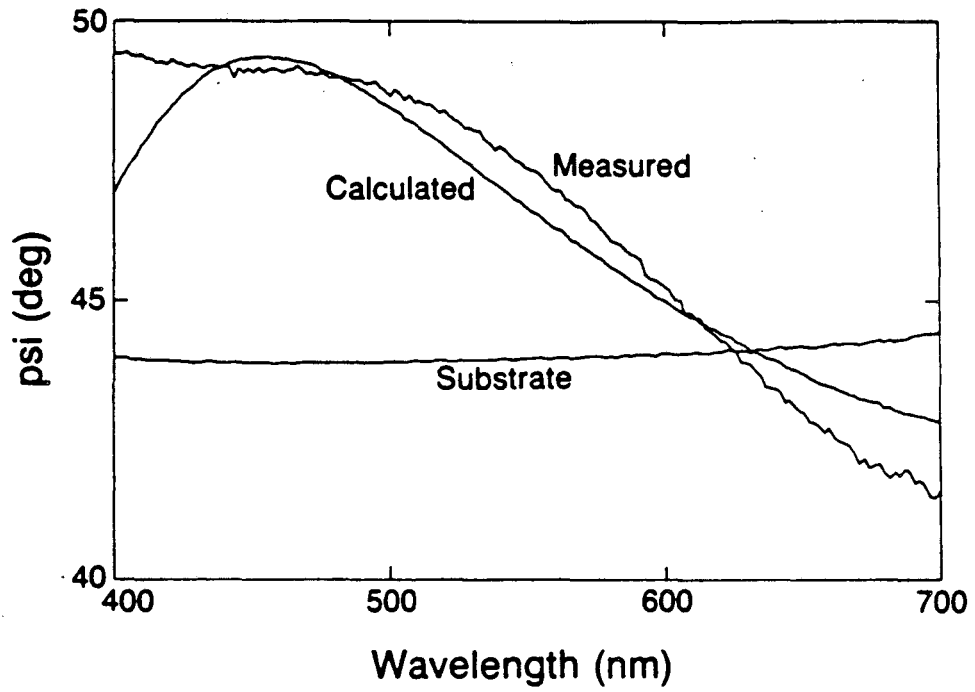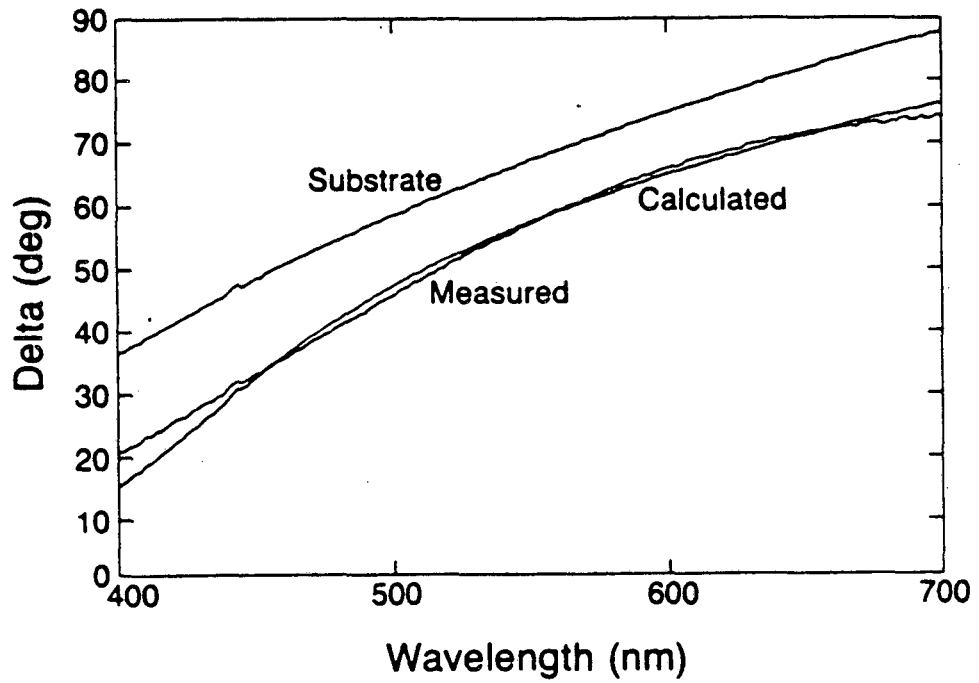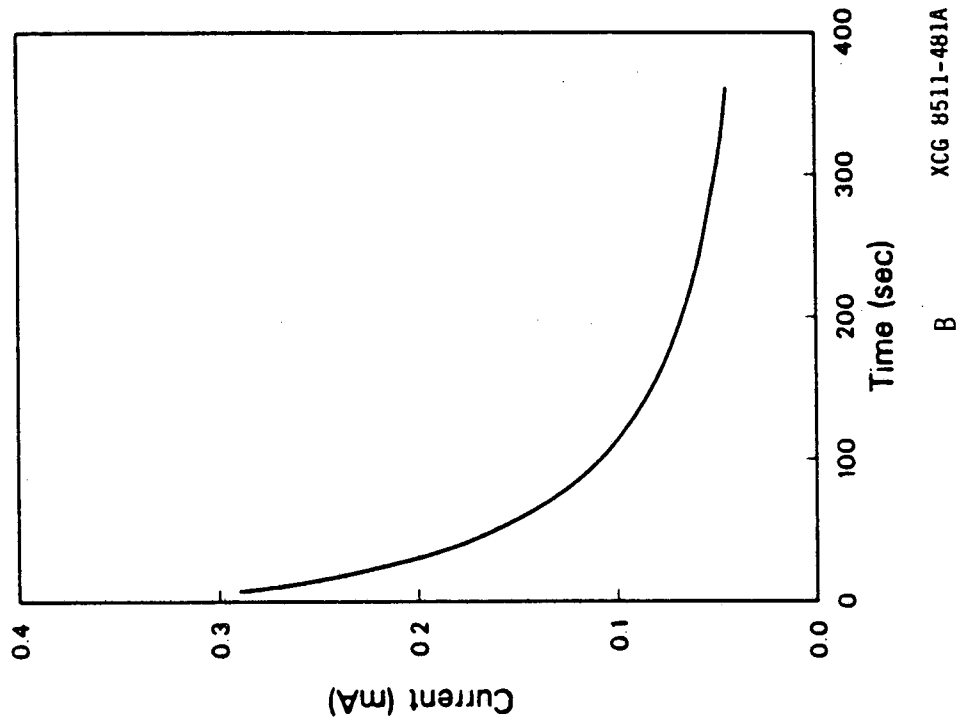


Fig. 10

XCG 8511-481A
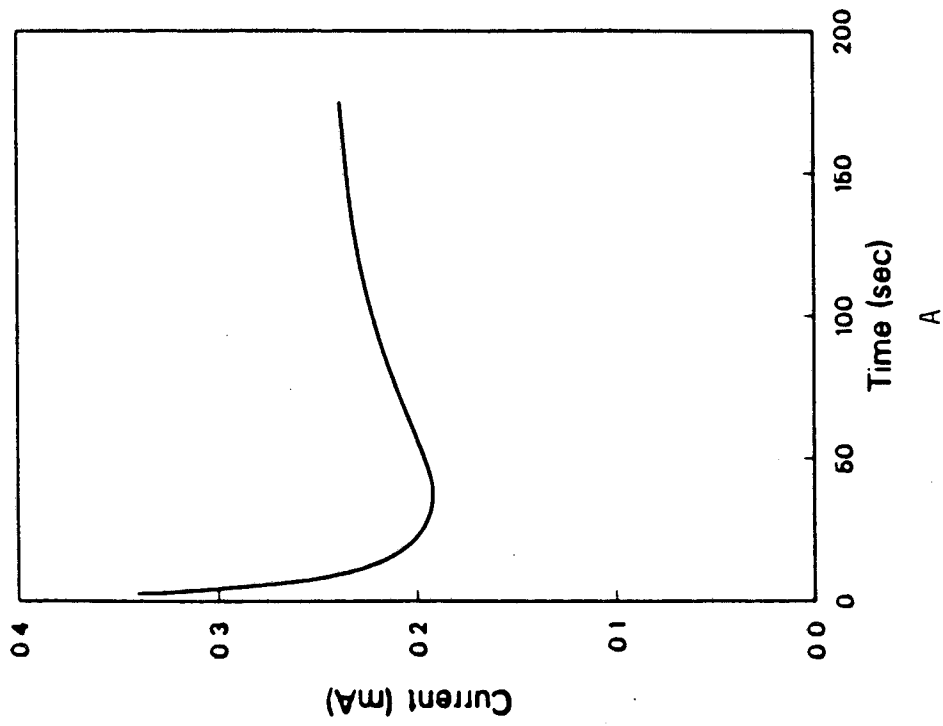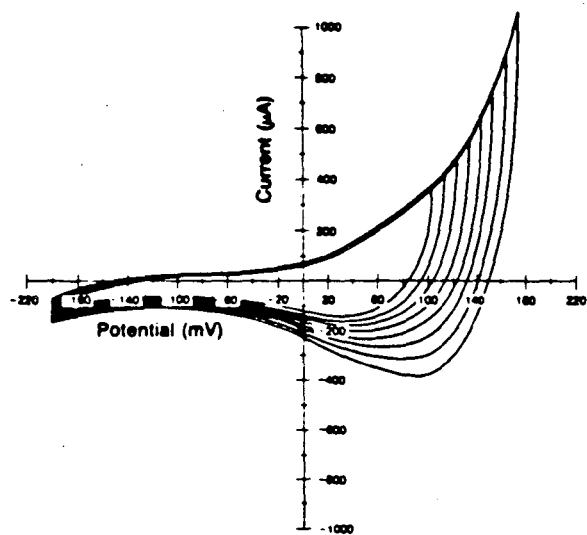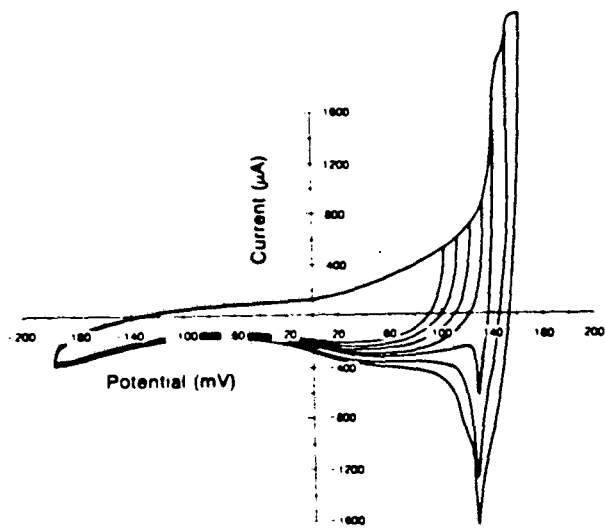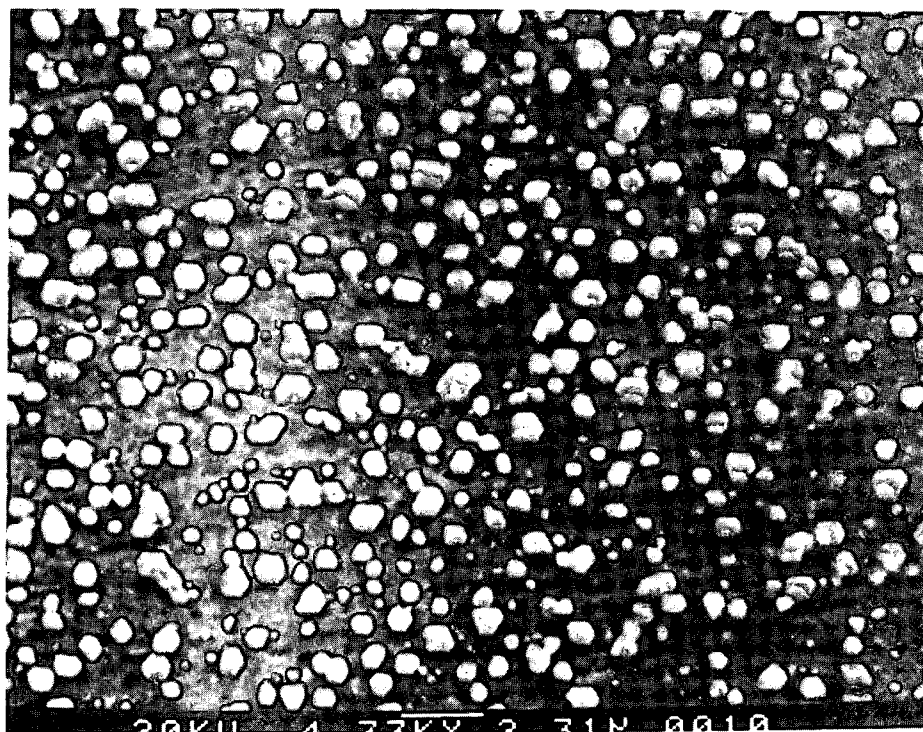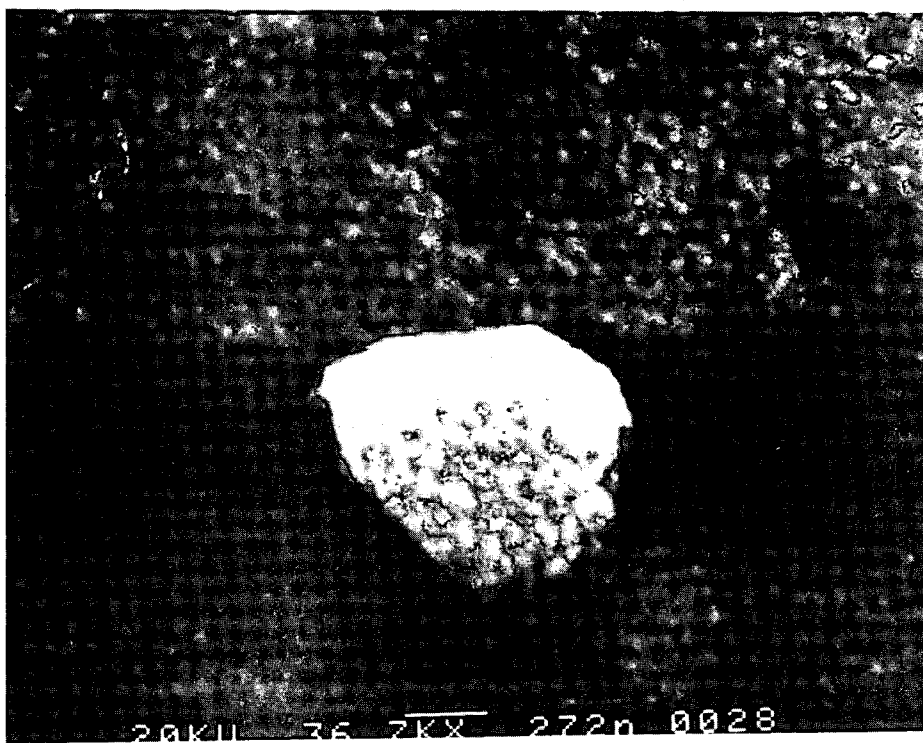
A
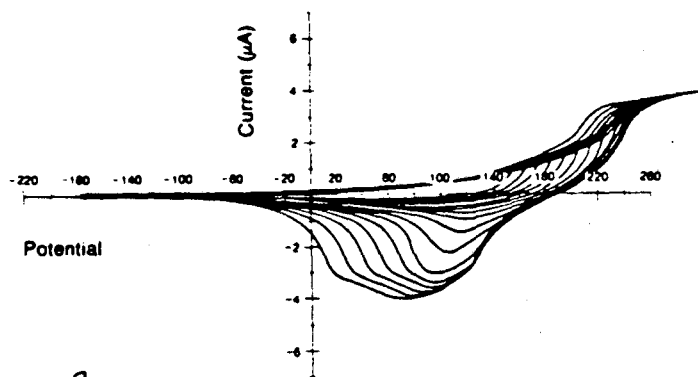
B

C

XBL 8511-11446A

Fig. 11

A
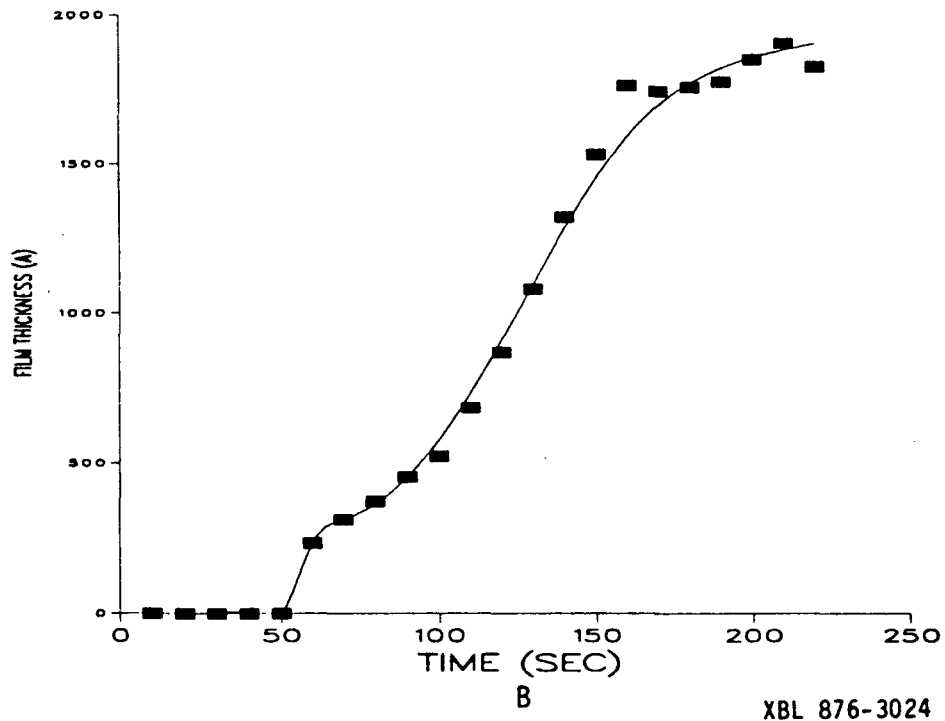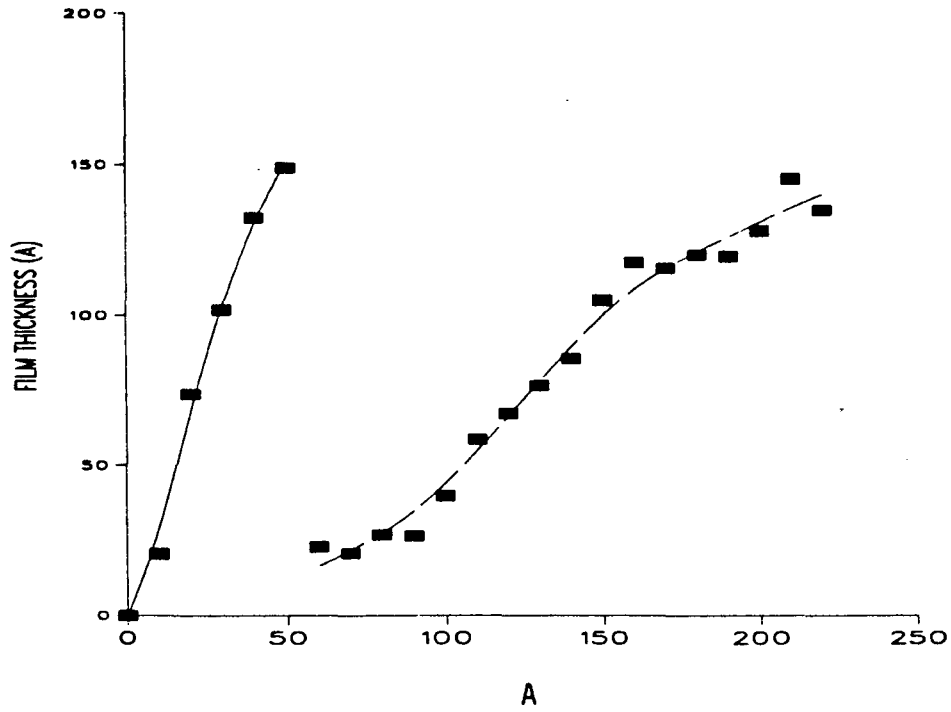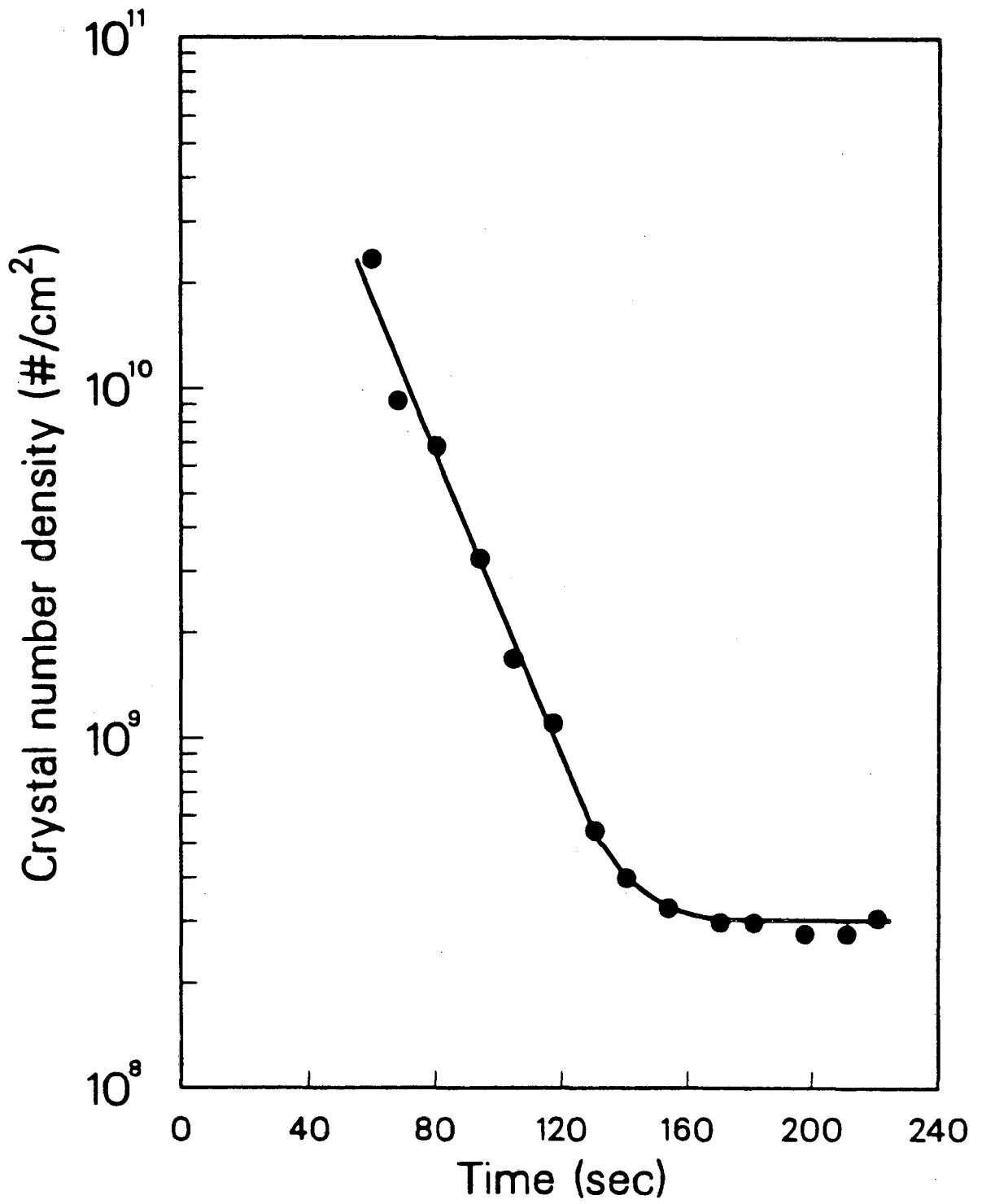
B

XBB859-7130A

Fig. 12

A

B

XBL 876-3024

Fig. 13
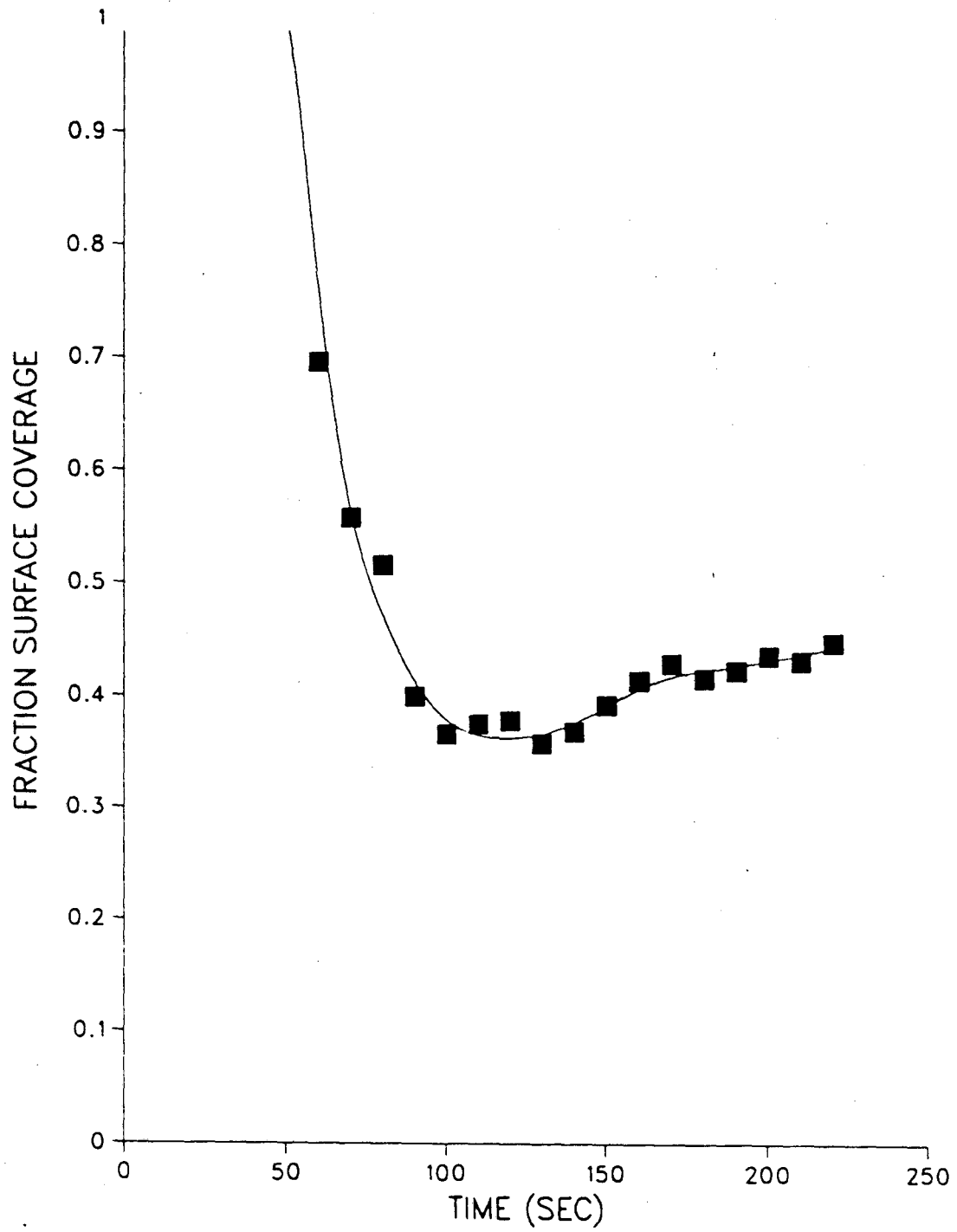
Fig. 14

XBL 876-3026
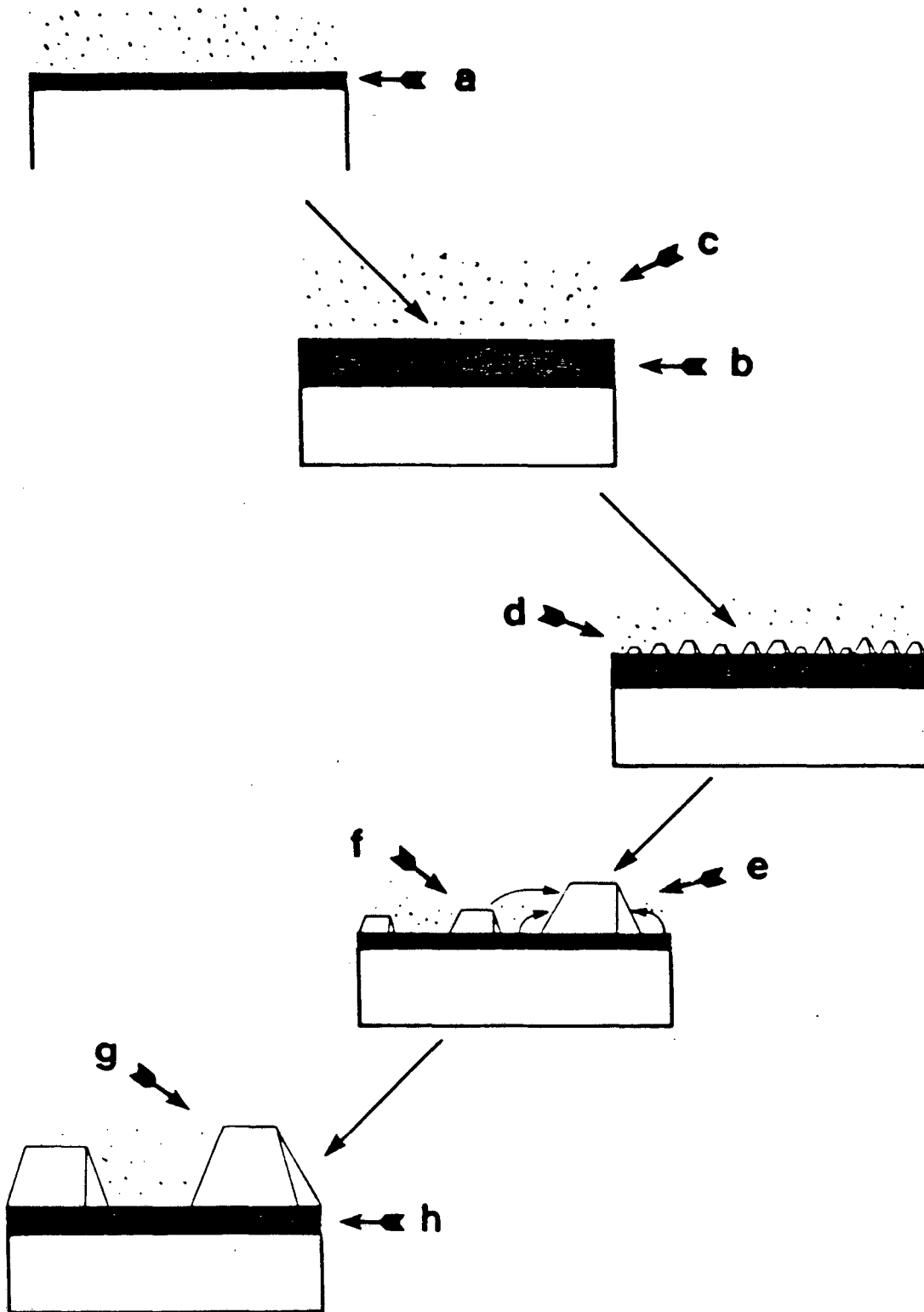
XCG 8512-544

Fig. 15

XBL 876-3025

Fig. 16

*LAWRENCE BERKELEY LABORATORY*
*TECHNICAL INFORMATION DEPARTMENT*
*UNIVERSITY OF CALIFORNIA*
*BERKELEY, CALIFORNIA 94720*